Galactic production of ^{138}La: Impact of ^{138,139}La statistical properties

B.V. Kheswa [a,b,*], M. Wiedeking [a], F. Giacoppo [c], S. Goriely [d], M. Guttormsen [c], A.C. Larsen [c], F.L. Bello Garrote [c], T.K. Eriksen [c], A. Görgen [c], T.W. Hagen [c], P.E. Koehler [c], M. Klintefjord [c], H.T. Nyhus [c], P. Papka [b], T. Renstrøm [c], S. Rose [c], E. Sahin [c], S. Siem [c], T. Tornyi [c]

[a] *iThemba LABS, P.O. Box 722, 7129 Somerset West, South Africa*
[b] *Physics Department, University of Stellenbosch, Private Bag X1, Matieland 7602, Stellenbosch, South Africa*
[c] *Department of Physics, University of Oslo, N-0316 Oslo, Norway*
[d] *Institut d'Astronomie et d'Astrophysique, Université Libre de Bruxelles, CP 226, B-1050 Brussels, Belgium*

ARTICLE INFO

ABSTRACT

The γ-ray strength functions and nuclear level densities of ^{138}La and ^{139}La have been measured below the neutron separation energies. These new data were used to calculate astrophysical Maxwellian-averaged (n, γ) cross-sections to investigate the production and destruction of the p-nucleus ^{138}La in the photodisintegration process. The results confirm the underproduction of ^{138}La in the p-process with respect to the observed abundances and strongly support the ν-process through ν_e capture on ^{138}Ba as the main contributor to the synthesis of ^{138}La in Type II supernovae.

1. Introduction

The major mechanisms to explain the synthesis of nuclei heavier than iron in the universe are: (a) the slow neutron-capture process (s-process), which occurs during the hydrostatic stellar burning phases of low-mass stars during their asymptotic giant branch phase [1] or of massive stars during core He-burning; (b) the rapid neutron-capture process (r-process) taking place in extremely high-neutron density environments [2]. The astrophysical sources and the specific conditions in which the r-process takes place are among the most longstanding mysteries of nuclear astrophysics. While the light r-process elements up to the first (or possibly second) abundance peak might be produced in neutrino-driven outflows of core-collapse supernovae [3–5], the decompression of cold neutronized matter from the violent collision of binary neutron stars or a neutron star with companion black holes have also been suggested as alternative sites [2,6–8].

Neutron capture processes can generally explain isotopic abundances with the notable exception of 35 p-nuclei which are stable or very long-lived systems with half-lives on the order of Gyr. Their production through the s- or r-processes is prohib-ited and they are instead synthesized in the p-process through photodisintegration reactions, i.e. (γ, n), (γ, p) or (γ, α), originating from seed nuclei which are created by the s- or r-processes [9] instead. The p-process can explain the observed solar abundances of most p-nuclei, with a few exceptions, one of them being ^{138}La [9–14]. ^{138}La is shielded from beta decay contributions by the stable isobars ^{138}Ce and ^{138}Ba, and photoreactions appear to be inefficient to produce ^{138}La significantly. The most promising theory brought forward for the synthesis of ^{138}La suggests that neutrinos from the proto-neutron star, created following the core-collapse, have enough intensity and energy to interact with matter through neutrino-induced reactions [13,15]. In particular the ^{138}Ba ν_e-capture has been calculated to be the largest contributor in the production of ^{138}La [10].

However, it was also clearly pointed out that nuclear physics properties, such as the nuclear level density (NLD) and γ-ray strength function (γSF), which are important ingredients in reaction rate calculations, are the main sources of uncertainty to evaluate the efficiency of the standard p-process mechanism [10]. The production of ^{138}La through ^{139}La$(\gamma, n)^{138}$La and its destruction by ^{138}La$(\gamma, n)^{137}$La are exclusively based on theoretical predictions. The NLD and γSF have never been measured for ^{138}La below the particle separation energy (S_n), which is the primary energy region of importance in the synthesis of ^{138}La. Data for ^{139}La are only available for excitation energies above 6 MeV [16]. Nuclear

* Corresponding author at: iThemba LABS, P.O. Box 722, 7129 Somerset West, South Africa.
E-mail address: bngkheswa@gmail.com (B.V. Kheswa).

physics parameters and their uncertainties need to be carefully measured in order to use them in model calculations to unambiguously exclude the standard p-process as the main contributor, and to confidently discuss the importance of neutrino interactions in the production of ^{138}La.

In this Letter, we report the measurements of the γ SF and NLD in ^{138}La and ^{139}La below S_n. These experimental results are subsequently used in reaction rate calculations to determine their impact on the observed abundances. The implications for the p- and ν_e-processes in the synthesis of ^{138}La will be addressed.

2. Experimental results

The seven-day experiment was conducted at the Oslo Cyclotron Laboratory with a ^{3}He beam of 38 MeV impinging on a 2.5 mg/cm^2 thick ^{139}La (99.9%) target. The beam intensity was kept in the range $\approx$0.4–0.7 pnA. Excited states in ^{138}La and ^{139}La nuclei were populated in the ^{139}La(^{3}He, ^{4}He) and ^{139}La(^{3}He, ^{3}He') reactions, respectively. Particles and γ-rays were measured in coincidence using the CACTUS (26 5″ × 5″ NaI detectors) and SiRi (64 ΔE-E telescopes with 130 μm thick ΔE and 1550 μm thick E detectors) arrays [17,18]. CACTUS is mounted on a spherical frame such that the target is located at the center with a distance of 22 cm from each NaI detector. The SiRi array was placed downstream, 50 mm from the target and covers a mean scattering angular range of 40–54°. During the analysis only the range 40–52° was used. The total efficiency and resolution of the CACTUS array are 14.1% and 7% FWHM for a 1332 keV transition, respectively. The particle telescopes have a resolution of $\approx$260 keV for the ^{3}He elastic peak. A 10.5 μm thick Al foil covers the front side of the particle telescopes to suppress δ-electrons.

The NaI detectors were calibrated with the 780.9 keV and 2759.1 keV γ-ray transitions in ^{27}Si which were produced in the ^{28}Si(^{3}He, ^{4}He)^{27}Si reaction. The excitation energy, E_x, of the ^{138}La and ^{139}La nuclei were obtained from the measured total energy of the ^{4}He and ^{3}He particles, corrected for kinematic effects, energy losses, and different Q-values. The particle-γ coincidence window was set to $\approx$50 ns by gating on the prompt time peak.

The Oslo Method [19,20] was used to extract the γ SF and NLD simultaneously. The E_x vs. E_γ matrices were constructed individually for ^{138}La and ^{139}La and have been unfolded with the CACTUS response matrix and the iterative technique discussed in [21]. The first generation matrices, $P(E_x, E_\gamma)$, were extracted (see Fig. 1) using the first generation method [22]. This iterative subtraction procedure reveals the distribution of the primary γ-rays for each initial excitation energy bin. The diagonal valley without data in Fig. 1(b) corresponds to the 1043 keV energy difference between the first- and second-excited states of ^{139}La. In the same figure two vertical regions corresponding to $E_\gamma \approx 1$ and 1.7 MeV are visible which are characterized by lower statistics due to over-subtraction of discrete and strong γ-ray transitions during the generation of $P(E_x, E_\gamma)$.

The NLD and γ SF are obtained from $P(E_x, E_\gamma)$ for both La nuclei under study. Assuming that the residual nucleus reaches a compound-like state before γ emission [23], and the Brink Hypothesis [24] is valid, $P(E_x, E_\gamma)$ can be factorized as [19],

$$P(E_x, E_\gamma) \propto \tilde{\rho}(E_f)\tilde{\mathcal{T}}(E_\gamma), \tag{1}$$

where $\tilde{\mathcal{T}}(E_\gamma)$ and $\tilde{\rho}(E_f)$ are the γ-ray transmission coefficient and level density at $E_f = E_x - E_\gamma$, respectively. Values for $\tilde{\mathcal{T}}(E_\gamma)$ and $\tilde{\rho}(E_f)$ were extracted by fitting theoretical first-generation matrices, $P_{th}(E_x, E_\gamma)$, to the experimental first-generation matrices $P(E_x, E_\gamma)$ individually for ^{138}La and ^{139}La. A χ^2 minimization between $P_{th}(E_x, E_\gamma)$ and $P(E_x, E_\gamma)$ using an iterative procedure
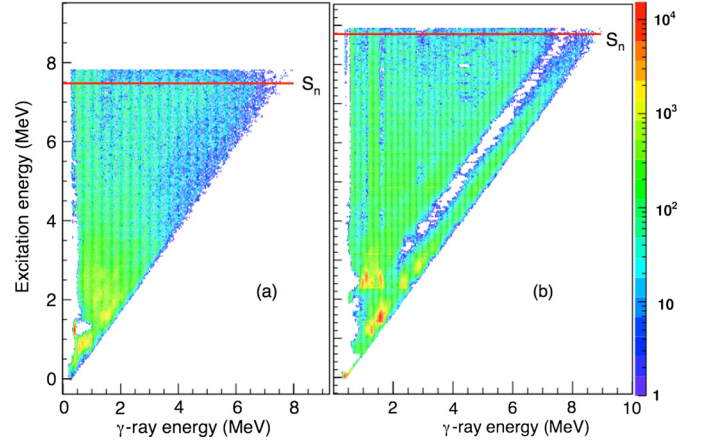

Fig. 1. (Color online.) The first-generation matrices, $P(E_x, E_\gamma)$, for ^{138}La (a) and ^{139}La (b). The neutron separation energies, S_n, are indicated by horizontal lines.

Table 1
Parameters used for the normalization of $\rho(E_x)$ and $f(E_\gamma)$ in ^{138,139}La.

Isotope	σ	D_0 (eV)	$\rho(S_n)$ (10^5 MeV^{-1})	$\langle\Gamma_\gamma(S_n)\rangle$ (meV)
^{138}La	6.9 ± 0.7^a	20.0 ± 4.4^b	7.1 ± 1.9^b	71.0 ± 13.6^b
^{139}La	5.5 ± 0.6^a	31.8 ± 7.0^c	2.9 ± 0.6^a	95.0 ± 18.2^c

^{a} Calculated with the HFB + Combinatorial model [25].
^{b} Estimated values (see text for details).
^{c} Average value from Refs. [28,29].

[19] determines the best fit, which was performed in the energy regions of $E_\gamma \geq 1$ MeV and 3.5 MeV $\leq E_x \leq 7.1$ MeV for ^{138}La, and $E_\gamma \geq 1.7$ MeV and 3.5 MeV $\leq E_x \leq 8.5$ MeV for ^{139}La, to exclude the non-statistical excitation energy regions.

Following extraction of $\tilde{\mathcal{T}}(E_\gamma)$ and $\tilde{\rho}(E_f)$, infinitely many solutions of $P(E_x, E_\gamma)$ can be found of the form,

$$\rho(E_f) = \tilde{\rho}(E_f) A e^{\alpha E_f} \tag{2}$$

$$\mathcal{T}(E_\gamma) = \tilde{\mathcal{T}}(E_\gamma) B e^{\alpha E_\gamma} \tag{3}$$

where α is the common slope for $\rho(E_f)$ and $\mathcal{T}(E_\gamma)$ and A and B are normalization parameters. Determination of α and A is accomplished by normalizing $\rho(E_f)$ to the level density at the neutron separation energy, $\rho(S_n)$, and at low excitation energies to the density of known discrete states. For ^{139}La, $\rho(S_n) = 2.9 \pm 0.6 \times 10^5$ MeV^{-1}, was used for normalization and was calculated from the experimental average neutron resonance level spacing, D_0 (see Table 1), using the Hartree–Fock–Bogoliubov (HFB) plus combinatorial model [25]. This value is in excellent agreement with $\rho(S_n) = 2.5 \pm 0.6 \times 10^5$ MeV^{-1} from the back shifted Fermi gas approach [26]. The absolute normalization parameter B is calculated using [20]:

$$\langle\Gamma_\gamma(S_n, J_T \pm \tfrac{1}{2}, \pi_T)\rangle = \frac{D_0}{4\pi} \int_0^{S_n} dE_\gamma \mathcal{T}(E_\gamma)\rho(S_n - E_\gamma)$$

$$\times \sum_{J=-1}^{1} g(S_n - E_\gamma, J_T \pm \tfrac{1}{2} + J) \tag{4}$$

where J_T, π_T are the spin and parity of the target nucleus in the (n, γ) reactions and $g(S_n - E_\gamma, J_T \pm \tfrac{1}{2} + J)$ is the spin distribution [20,27] which is normalized to $\sum_J g(E_x, J) \approx 1$. For ^{139}La $\langle\Gamma_\gamma(S_n, J_T, \pi_T)\rangle$, and D_0 are available experimental values, and averaged from Refs. [28,29]. Their respective uncertainties were obtained with appropriate error propagation. However, for ^{138}La
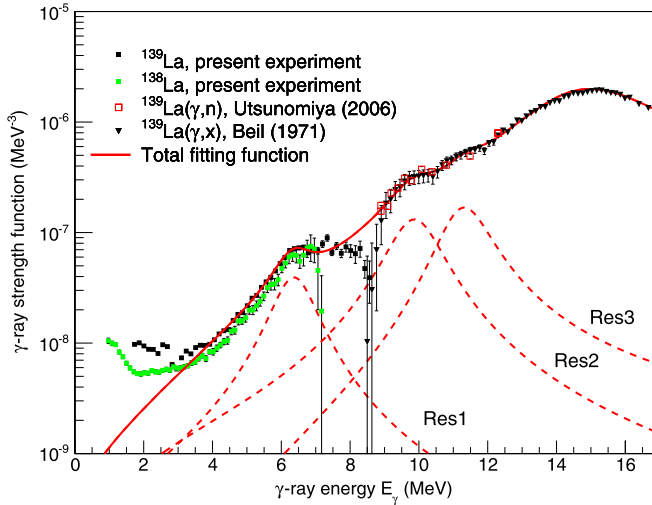
Fig. 2. (Color online.) Comparison of $f(E_\gamma)$ with photoneutron cross-section data. "Res1", "Res2", and "Res3" indicate the fits to individual resonance structures for ^{139}La, while $f(E_\gamma)$ for ^{138}La is included for comparison.

Table 2
Lorentzian parameters used in the fit to the experimental data, where E_0, σ_0, and Γ_0 are the centroid energies, cross sections, and widths of the resonance peaks, respectively.

Resonance	E_0 (MeV)	σ_0 (mb)	Γ_0 (MeV)
Res1	6.4	2.9	1.3
Res2	9.9	15	1.6
Res3	11.4	15	1.4
GEDR	15.6[a]	336	5.6[a]

[a] Modified from Ref. [28] (see text for details).

parameters were somewhat increased from Ref. [28] to obtain the best fit to the experimental data, while for other resonances they were directly determined from the fit to the data.

3. Discussion

Overall, the present data exhibit very good agreement with the extrapolated tail of the GEDR data of Refs. [36,37]. The resonance at $E_\gamma = 6.4$ MeV is consistent with previous measurements [16] where its origin has been discussed to be an E1 pygmy resonance. Moreover, the measured $f(E_\gamma)$ exhibits a plateau behavior between 2 and 4 MeV for both La isotopes and a pronounced enhancement for $E_\gamma < 1.7$ MeV for ^{138}La. Data for ^{139}La could not be extracted below 1.7 MeV due to the exclusion of this region as discussed in Section 2. This low-energy enhancement has been observed in previous studies of light- to medium-mass nuclei using the Oslo Method (^{44,45}Sc [38], ^{50,51}V [39], ^{44,45,46}Ti [40–42], ^{56,57}Fe [35], $^{93–98}$Mo [43]) with the possible transitional region reported in ^{105,106}Cd [26]. The existence of the low-energy enhancement has been independently confirmed using a different experimental setup and extraction technique for ^{95}Mo [44]. The unexpected appearance of the enhancement in ^{138}La suggests that this feature is not confined to specific mass regions but may be found across the nuclear chart.

No conclusive theoretical interpretation exists which can explain these observations although different models have suggested that the low-energy enhancement may be due to: 1) transitions within the single-particle continuum producing E1 radiation [45], and 2) a reorientation of the spins of high-j neutron and proton orbits producing M1 transitions [46]. It is intriguing to note that ^{138}La is located within a predicted region of magnetic rotation [47], consistent with the theoretical approach 2).

To estimate the ^{137,138}La radiative neutron capture cross sections and the corresponding reverse photoneutron emission rates of astrophysical interest, statistical model calculations were carried out using the TALYS code [30,48]. Some of the principal ingredients of these calculations are the γSF and the NLD. As far as the strength function is concerned, the new experimental results, which provide a direct measurement of the γSF up to the neutron threshold, are now considered and entered directly in the TALYS calculation of the electromagnetic transmission coefficient. For incident neutron energies, typically below 1 MeV, it is found that the energy window giving rise to the dominant contribution to the neutron capture cross section corresponds to photon energies of about 3 to 7 MeV, i.e. energies at which the γSFs have now been determined experimentally (Fig. 2). In such conditions, and consequently for energies of astrophysical relevance, the extra low-lying strength found around 6.4 MeV (Fig. 2) is expected to affect the cross section predictions.

The uncertainties of the γSFs were modified with the upper error bars obtained by replacing D_0 by $D_0 - \Delta D_0$ and $\langle\Gamma_\gamma(S_n, J_T, \pi_T)\rangle$ by $\langle\Gamma_\gamma(S_n, J_T, \pi_T)\rangle + \Delta\langle\Gamma_\gamma(S_n, J_T, \pi_T)\rangle$ during the normalization of γSF. The lower error bars of the γSFs were obtained by replacing D_0 by $D_0 + \Delta D_0$ and $\langle\Gamma_\gamma(S_n, J_T, \pi_T)\rangle$ by
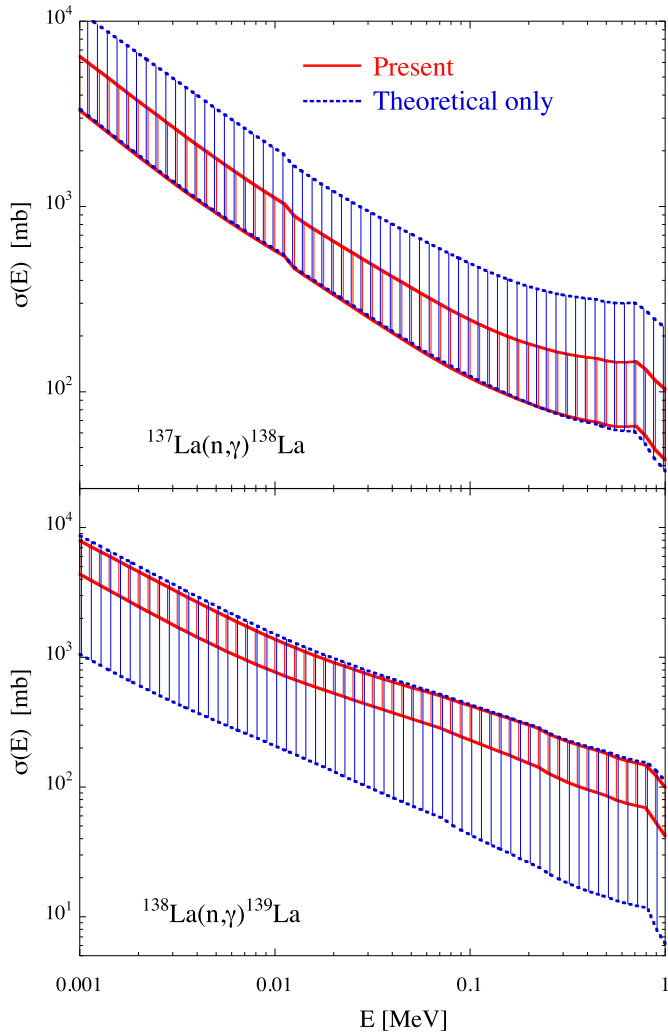
there are neither D_0 nor $\langle\Gamma_\gamma(S_n, J_T, \pi_T)\rangle$ experimental values available in the literature. Therefore, the value of $\langle\Gamma_\gamma(S_n, J_T, \pi_T)\rangle$ was estimated from a spline fit as implemented in the TALYS reaction code [30], while $\rho(S_n)$ was estimated by normalizing $\rho(E_f)$ and $\mathcal{T}(E_\gamma)$ of ^{138}La with the requirement of having the same slope as $\rho(E_f)$ and $\mathcal{T}(E_\gamma)$ in ^{139}La. It is expected that $\rho(E_f)$ and $\mathcal{T}(E_\gamma)$ of neighboring isotopes have the same slope [26,31,32]. The resulting value for $\rho(S_n)$ is then used to calculate D_0 for ^{138}La with [20],

$$\rho(S_n) = \frac{2\sigma^2}{D_0(J_T + 1)e^{[-(J_T+1)^2/2\sigma^2]} + e^{(-J_T^2/2\sigma^2)}J_T}, \quad (5)$$

where σ is the spin cut-off parameter at S_n. Furthermore, the estimation of $\langle\Gamma_\gamma(S_n)\rangle$ for ^{138}La with the TALYS code does not provide uncertainty, $\Delta\langle\Gamma_\gamma(S_n)\rangle$, and this value was computed by assuming the same percentage uncertainty as for the neighboring isotope, ^{139}La. The estimated uncertainty is further supported by the (γ, n) data and the similarity to the ^{139}La γSF. This approach has been used for some Mo isotopes [33], and is also used to calculate ΔD_0. The parameters which were used for the normalization of $\rho(E_f)$ and $\mathcal{T}(E_\gamma)$ are summarized in Table 1.

With the assumption, strongly supported by experimental data [34,35], that statistical decay is dominated by dipole transitions, the γSF, $f(E_\gamma)$ can be calculated from $\mathcal{T}(E_\gamma)$ using

$$f(E_\gamma) = \frac{\mathcal{T}(E_\gamma)}{2\pi E_\gamma^3}. \quad (6)$$

Fig. 2 shows $f(E_\gamma)$ for ^{139}La together with data extracted from the ^{139}La(γ, n) and ^{139}La(γ, x) cross-sections [36,37]. The $f(E_\gamma)$ for ^{138}La has also been included for comparison. For ^{139}La the giant electric dipole resonance (GEDR) at $E_\gamma \approx 15.6$ MeV was fitted with an enhanced generalized Lorentzian function, f^{EGLO} [34] and a constant nuclear temperature of $T_f = 0.1$ MeV which was considered as a free parameter. The excess strengths at $E_\gamma \approx 11.4$ ("Res3" in Fig. 2) and 9.9 MeV ("Res2" in Fig. 2) were fitted with the standard Lorentzian function, f^{SLO} [34]. In addition, an enhancement in the strength of ^{139}La at $E_\gamma \approx 6.4$ MeV is observed. In Fig. 2 this resonance is described using the f^{SLO} and labeled as "Res1". The total ^{139}La fitting function is given by $f(E_\gamma) = f^{EGLO}_{GEDR}(E_\gamma, T_f = 0.1$ MeV$) + f^{SLO}_{Res3}(E_\gamma) + f^{SLO}_{Res2}(E_\gamma) + f^{SLO}_{Res1}(E_\gamma)$. The Lorentzian parameters used in this fit are listed in Table 2. For the GEDR the

Fig. 3. (Color online.) Upper panel: ^{137}La$(n, \gamma)^{138}$La cross section as a function of neutron energy. The red solid lines are obtained with the present measured γSF, while the dashed blue lines are derived from theoretical models of γSF and NLD without any constraints on experimental values. Lower panel: Same for ^{138}La$(n, \gamma)^{139}$La (solid line) cross sections. See text for more details.

$\langle \Gamma_\gamma (S_n, J_T, \pi_T) \rangle - \Delta \langle \Gamma_\gamma (S_n, J_T, \pi_T) \rangle$. For ^{138}La the uncertainties in γSF are $^{+52}_{-34}$% at $E_\gamma = 7.2$ MeV, gradually decreasing to $^{+15}_{-17}$% at $E_\gamma = 1.0$ MeV, while for ^{139}La the ranges are $^{+69}_{-39}$% at $E_\gamma = 8.6$ MeV, decreasing to ± 15% at $E_\gamma = 1.7$ MeV. NLDs also play an important role in the calculation of the radiative capture cross section. The NLDs calculated with the HFB plus combinatorial model [25] and normalized to the experimental cumulative number of low-lying states as well as the s-wave resonance spacing (with their corresponding error bars) at S_n (see Table 1), is in general agreement with the experimental extracted values of $\rho(E_f)$ (to be published elsewhere), and is used in the present calculation.

The final neutron capture cross sections, $\sigma(E)$, including the uncertainties affecting the γSF and the NLD (Table 1), are given in Fig. 3. Despite the remaining uncertainties affecting both the experimental γSF and theoretical NLD (Table 1), the radiative neutron cross sections are significantly better constrained when compared to the predictions based on theoretical ingredients only. We show in Fig. 3 the cross sections obtained with the TALYS code considering theoretical γSF and NLD models only. More specifically, we include 6 different NLD models, namely back-shifted

Fermi gas models [49], the Generalized Superfluid model [50] and mean field plus statistical [51] or combinatorial models [25, 52], and 6 different γSF prescriptions of both the Lorentzian-type [53–55] and mean field plus Quasi-Random Phase Approximation [56–58]. These various γSF and NLD models allow us to estimate the model uncertainties affecting the predicted cross section when no experimental data exist to constrain the γSF. In addition, some parameter uncertainties have been considered to allow for possible variations of the various parameters entering such models. The corresponding upper and lower limits resulting from such model and parameter uncertainties illustrate the present predictive power of the reaction model and are seen in Fig. 3 to give rise to cross sections that are significantly less constrained in comparison with the newly determined cross sections based on the present experiment. It should also be stressed that these theoretical-only cross sections are obtained with nuclear models that are extrapolated to ^{138}La and ^{139}La on the basis of existing models tuned on available experimental data [59] and that the possible existence of a strong E1 resonance or unknown structures in γSF or NLD that are not predicted by present models could not be excluded. While larger uncertainties could have been envisioned if justified by theory or experiments, our new experimental results show that such unexpected patterns in the γSF can be excluded and furthermore provide directly the γSF in the energy region of interest. However, non-negligible uncertainties still affect the NLD predictions, those dominate the remaining uncertainties on the cross sections.

The astrophysical Maxwellian-averaged cross sections (MACS) estimated with the newly determined γSF amount to $\langle \sigma \rangle = 366 \pm 126$ mb and 116 ± 44 mb for ^{137}La$(n, \gamma)^{138}$La at the s-process thermal energy of $kT = 30$ keV (i.e. a temperature of $T = 3.5 \times 10^8$ K) and at the p-process energy of 215 keV ($T = 2.5 \times 10^9$ K), respectively. For ^{138}La$(n, \gamma)^{139}$La, we obtain $\langle \sigma \rangle = 618 \pm 174$ mb and 54 ± 20 mb at $T = 3.5 \times 10^8$ K and 2.5×10^9 K, respectively. The ^{138}La$(n, \gamma)^{139}$La cross section at $T = 3.5 \times 10^8$ K is about 45% larger than the compiled theoretical value [60]. At $T = 2.5 \times 10^9$ K, the MACS are close (within less than 15%) to the values of 123 mb and 62 mb derived in Ref. [10] for ^{137}La and ^{138}La, respectively. From these derived cross sections, it can already be deduced [10] that the synthesis of ^{138}La through photodisintegration processes cannot be efficient enough to reproduce observed abundances. Moreover, with respect to theoretical only predictions, as described above, the MACS is better constrained. More specifically, for the various unconstrained γSF and NLD models considered here, the ^{137}La$(n, \gamma)^{138}$La cross section at $T = 3.5 \times 10^8$ K would fall in the large range of 620 ± 370 mb and the ^{138}La$(n, \gamma)^{139}$La cross section of 465 ± 365 mb. Previous theoretical calculations predicted the ^{138}La$(n, \gamma)^{139}$La MACS at $T = 3.5 \times 10^8$ K in the range of 194 to 781 mb [61].

To confirm the impact of the new rates on the ^{138}La p-process production, nucleosynthesis in the O/Ne-rich layers of type II supernovae for a solar metallicity star of $25 M_\odot$ was performed, in absence of neutrino nucleosynthesis (more details can be found in Refs. [2,10]; note, however, that theoretical rates are determined here using the TALYS code [30,48]). The resulting overproduction factors, $\langle F \rangle$, (with respect to the solar abundances) in the $0.75 M_\odot$ p-process layers are shown in Fig. 4 where the upper and lower limits on the ^{138}La abundance are obtained with the newly derived reaction rates (Fig. 3). For comparison, we also include the ^{138}La overproduction factors obtained when considering the theoretical-only MACS obtained without considering the new experimental constraints. Though the new cross section determination tends to confirm the largest abundances of ^{138}La obtained with the upper values of the theoretical-only MACS, ^{138}La remains underproduced by a factor of about 10 with respect to the neighboring p-nucleus ^{138}Ce. The new determination of the reaction rates with the im-
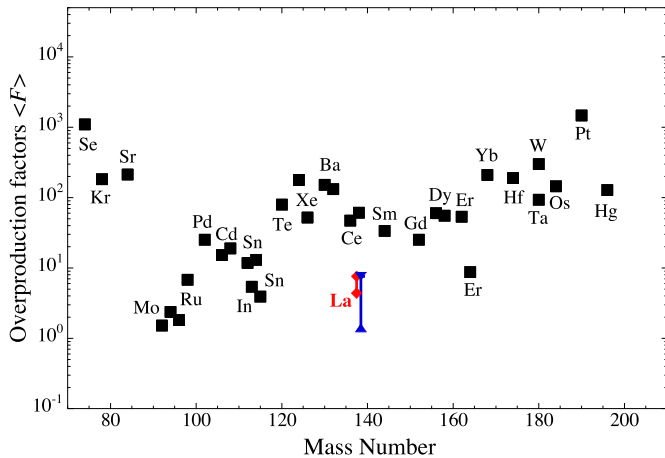
Fig. 4. (Color online.) *P*-nuclide overproduction factors $\langle F \rangle$ in the $0.75\,M_\odot$ *p*-process layers of a $25\,M_\odot$ type II supernovae as a function of the mass number *A*. The maximum and minimum ^{138}La abundances are obtained on the basis of the upper and lower limits (Fig. 3) of the newly determined reaction rates (red diamonds) or of the theoretical only rates (blue triangles).

proved γSFs therefore does not give more room for a possible strong production of ^{138}La and confirms the previous conclusions that ^{138}La cannot be sufficiently produced by photoreactions during the standard *p*-process. This result, together with theoretical predictions [10,14] puts the ν_e-process as the dominant production process for ^{138}La on a very strong footing.

4. Summary

The γSF and NLD of ^{138}La and ^{139}La have been measured with the Oslo Method. The γSF of ^{138}La exhibits a low-energy enhancement, the first such observation in such a heavy system. Experimental results were used to calculate the neutron capture cross sections of 116 ± 44 mb for ^{137}La$(n,\gamma)^{138}$La and 54 ± 20 mb for ^{138}La$(n,\gamma)^{139}$La at the *p*-process energy of 215 keV. Despite these new cross sections a significant underproduction of ^{138}La in the *p*-process still exists. These results support the ν_e-process as the primary reaction to synthesize ^{138}La to the observed solar abundance levels.

Acknowledgements

References

[1] O. Straniero, et al., Nucl. Phys. A 777 (2006) 311.
[2] M. Arnould, et al., Phys. Rep. 450 (2007) 97.
[3] S. Wanajo, et al., Astrophys. J. Lett. 726 (2011) L15.
[4] H.-T. Janka, Annu. Rev. Nucl. Part. Sci. 62 (2012) 407.
[5] A. Arcones, et al., J. Phys. G, Nucl. Part. Phys. 41 (2014) 044005.
[6] S. Goriely, et al., Astrophys. J. Lett. 738 (2011) L32.
[7] A. Bauswein, et al., Astrophys. J. 773 (2013) 78.
[8] S. Rosswog, et al., Mon. Not. R. Astron. Soc. 439 (2014) 744.
[9] M. Arnould, S. Goriely, Phys. Rep. 384 (2003) 1.
[10] S. Goriely, et al., Astron. Astrophys. 375 (2001) L35.
[11] T. Rauscher, in: Proceedings of Science, SISSA, 2011, p. 059.
[12] T. Rauscher, et al., Rep. Prog. Phys. 76 (2013) 066201.
[13] S.E. Woosley, et al., Astrophys. J. 356 (1990) 272.
[14] A. Heger, et al., Phys. Lett. B 606 (2005) 258.
[15] T. Kajino, et al., J. Phys. G, Nucl. Part. Phys. 41 (2014) 044007.
[16] A. Makinaga, et al., Phys. Rev. C Nucl. Phys. 82 (2010) 024314.
[17] M. Guttormsen, et al., Nucl. Instrum. Methods Phys. Res., Sect. A, Accel. Spectrom. Detect. Assoc. Equip. 648 (2011) 168.
[18] M. Guttormsen, et al., Phys. Scr. T 32 (1990) 54.
[19] A. Schiller, et al., Nucl. Instrum. Methods Phys. Res., Sect. A, Accel. Spectrom. Detect. Assoc. Equip. 447 (2000) 498.
[20] A.C. Larsen, et al., Phys. Rev. C 83 (2011) 034315.
[21] M. Guttormsen, et al., Nucl. Instrum. Methods Phys. Res., Sect. A, Accel. Spectrom. Detect. Assoc. Equip. 374 (1996) 371.
[22] M. Guttormsen, et al., Nucl. Instrum. Methods Phys. Res., Sect. A, Accel. Spectrom. Detect. Assoc. Equip. 255 (1987) 518.
[23] A. Bohr, B. Mottelson, Nuclear Structure, vol. I, Benjamin, New York, 1969.
[24] D.M. Brink, Ph.D. thesis, Oxford University, 1955, pp. 101–110.
[25] S. Goriely, S. Hilaire, A.J. Koning, Phys. Rev. C Nucl. Phys. 78 (2008) 064307.
[26] A.C. Larsen, et al., Phys. Rev. C 87 (2013) 014319.
[27] T. von Egidy, D. Bucurescu, Phys. Rev. C 80 (2009) 054310.
[28] R. Capote, et al., Reference input parameter library, RIPL-2 and RIPL-3; available online at: http://www-nds.iaea.org/RIPL-3/.
[29] S.F. Mughabghab, Atlas of Neutron Resonances, 5th ed., Elsevier Science, Amsterdam, 2006.
[30] A.J. Koning, et al., in: O. Bersillon, et al. (Eds.), Nuclear Data for Science and Technology, EDP Sciences, 2008, p. 211, see also http://www.talys.eu.
[31] S. Siem, et al., Phys. Rev. C 65 (2002) 044318.
[32] H.T. Nyhus, et al., Phys. Rev. C 85 (2012) 014323.
[33] H. Utsunomiya, et al., Phys. Rev. C 88 (2013) 015805.
[34] J. Kopecky, M. Uhl, Phys. Rev. C 41 (1990) 1941.
[35] A.C. Larsen, et al., Phys. Rev. Lett. 111 (2013) 242504.
[36] H. Utsunomiya, et al., Phys. Rev. C 74 (2006) 025806.
[37] H. Beil, et al., Nucl. Phys. A 172 (1971) 426.
[38] A.C. Larsen, et al., Phys. Rev. C 76 (2007) 044303.
[39] A.C. Larsen, et al., Phys. Rev. C 73 (2006) 064301.
[40] A.C. Larsen, et al., Phys. Rev. C 85 (2012) 014320.
[41] N.U.H. Syed, et al., Phys. Rev. C 80 (2009) 044309.
[42] M. Guttormsen, et al., Phys. Rev. C 83 (2011) 014312.
[43] M. Guttormsen, et al., Phys. Rev. C 71 (2005) 044307.
[44] M. Wiedeking, et al., Phys. Rev. Lett. 108 (2012) 162503.
[45] E. Litvinova, N. Belov, Phys. Rev. C 88 (2013) 031302(R).
[46] R. Schwengner, S. Frauendorf, A.C. Larsen, Phys. Rev. Lett. 111 (2013) 232504.
[47] S. Frauendorf, Rev. Mod. Phys. 73 (2001) 463.
[48] S. Goriely, et al., Astron. Astrophys. 487 (2008) 467.
[49] A.J. Koning, S. Hilaire, S. Goriely, Nucl. Phys. A 810 (2008) 13.
[50] A.V. Ignatyuk, Rep. INDC(CCP)-233, International Atomic Energy Agency, Vienna, Austria, 1985.
[51] P. Demetriou, S. Goriely, Nucl. Phys. A 695 (2001) 95.
[52] S. Hilaire, M. Girod, S. Goriely, A.J. Koning, Phys. Rev. C 86 (2012) 064317.
[53] P. Axel, Phys. Rev. 126 (1962) 671.
[54] J. Kopecky, M. Uhl, Phys. Rev. C 41 (1990) 1941.
[55] S. Goriely, Phys. Lett. B 436 (1998) 10.
[56] S. Goriely, E. Khan, Nucl. Phys. A 706 (2002) 217.
[57] S. Goriely, M. Samyn, E. Khan, Nucl. Phys. A 739 (2004) 331.
[58] I. Daoutidis, S. Goriely, Phys. Rev. C 86 (2012) 034328.
[59] R. Capote, et al., Nucl. Data Sheets 110 (2009) 3107.
[60] Z.Y. Bao, et al., At. Data Nucl. Data Tables 76 (2000) 70.
[61] The Karlsruhe Astrophysical Database of Nucleosynthesis in Stars, August 2014; available online at: http://exp-astro.physik.uni-frankfurt.de/kadonis1.0/.